International Journal of Remote Sensing
Vol. 33, No. 23, 10 December 2012, 7559–7578

Adaptive retracking of Jason-1 altimetry data for inland waters: the example of the Gorky Reservoir

YULIYA TROITSKAYA*†‡, GALINA RYBUSHKINA†, IRINA SOUSTOVA†, GALINA BALANDINA†, SERGEY LEBEDEV§¶ and ANDREY KOSTIANOY|

†Institute of Applied Physics RAS, Nizhny Novgorod, Russia
‡Obukhov Institute of Atmospheric Physics RAS, Moscow, Russia
§Geophysical Centre of RAS, Moscow, Russia
¶Space Research Institute RAS, Moscow, Russia
|P.P. Shirshov Institute of Oceanology RAS, Moscow, Russia

(*Received 29 November 2010; in final form 9 March 2012*)

Standard altimetry data processing developed for open ocean conditions can be inapplicable for the case of inland waters, especially for narrow, elongated waterbodies and rivers, where the distance between shores is less than 10 km (while the eliminated area within the gain of the radar antenna for Jason-1,2 is about 50 km). These conditions are typical, for example, of the majority of reservoirs of the Volga River cascade (with one exception: the Rybinskoe Reservoir). Under these conditions only a few telemetric impulses fit the validity criteria, which causes a severe loss of data. Besides, errors in the water level retrieved from the altimetric measurements are enormous, as was demonstrated on the basis of comparison of *in situ* measurements at hydro-gauging stations for the water level of the Gorky Reservoir of the Volga River and all that is available along track 10 Hz TOPEX/Poseidon altimetry data and 20 Hz Jason altimetry data over the reservoir area.

The problem of minimization of the errors can be resolved by retracking. For justification of the optimal retracking algorithm, the average impulse response of the statistically inhomogeneous surface was calculated theoretically, based on the works of Brown (1977) and Barrick and Lipa (1985) for the model of the terrain in the vicinity of the Gorky Reservoir. The model represents the main typical features of the waveform examples (e.g. high peaks or irregular complex shape), and the modelled waveforms are in good agreement with the Jason-1,2 waveforms for the same area. It was shown that for the Gorky Reservoir significant wave height (SWH) did not exceed 0.5 m (corresponding to the width of the leading edge less than 1 telemetric gate). Under these conditions the retracking algorithm based on the detection of the beginning of the leading edge of telemetric impulses is preferable for a correct assessment of variations in the water level in the Gorky Reservoir.

A comparison of the data with *in situ* measurements at the hydro-gauging stations for the water level of the Gorky Reservoir shows that retracking dramatically increases the number of data involved in monitoring and significantly improves the accuracy of the measurement of the water level. The retracked data of water level have also been validated by comparing them with Jason-2 and Jason-1 after carrying out measurements for the Gorky Reservoir. The general principles of retracking

*Corresponding author. Email: yuliya@hydro.appl.sci-nnov.ru

International Journal of Remote Sensing
ISSN 0143-1161 print/ISSN 1366-5901 online © 2012 Taylor & Francis
http://www.tandfonline.com
http://dx.doi.org/10.1080/01431161.2012.685972

algorithms for complex areas (land, coastal zone, inland waters, etc.), based on calculations of the waveform and taking into account statistical inhomogeneity of the reflecting surface adjusted to a certain geographic region, are discussed.

1. Introduction

Altimetry data processing algorithms developed for an open ocean may be inapplicable for the cases of coastal and inland waters. The problems of inland water data processing are very similar to those arising for the coastal zone of an ocean from contamination of the received signal by reflection from the land. This effect is very strong in the Gorky Reservoir with a maximum width of 14 km and steep 10–20 m banks. Under these conditions few telemetric pulses fit the validity criterion, which causes considerable data loss. As a result, the Gorky Reservoir is not included in the databases of Laboratoire d'Etudes en Géophysique et Océanographie Spatiales (LEGOS) and the US Department of Agriculture's Foreign Agricultural Service. This work is about retrieving the water level data for the Gorky Reservoir by an adaptive retracking algorithm, which dramatically increases the amount of data involved in monitoring. The general principles of the considered regional retracking algorithm may be useful for altimetry of other cases of inland waterbodies and coastal zones.

2. Features of inland water altimetry: fundamentals of the method of adaptive regional retracking

In the coastal zone, altimeter waveforms differ significantly from those formed in an open ocean. This occurs due to the impact of land reflection. Figure 1 shows examples of telemetric waveforms generated by reflection from land and water (figure 1(*a*)), quasi-specular coherent reflection from a smooth water surface in estuaries and harbours (figure 1(*b*)) and other highly reflective objects (coastal buildings, large slick areas, etc., see figure 1(*c*)).

In the presence of additional peaks, the waveform is poorly approximated by Brown's formula (Brown 1977), which leads to errors in determining the position of the leading edge and, hence, to a wrong determination of satellite altitude and water level, when the Brown-like formula based algorithms are applied. In this case, the other quantities, such as wind speed and significant wave height (SWH) are also determined incorrectly. In this regard, recently special algorithms have been actively

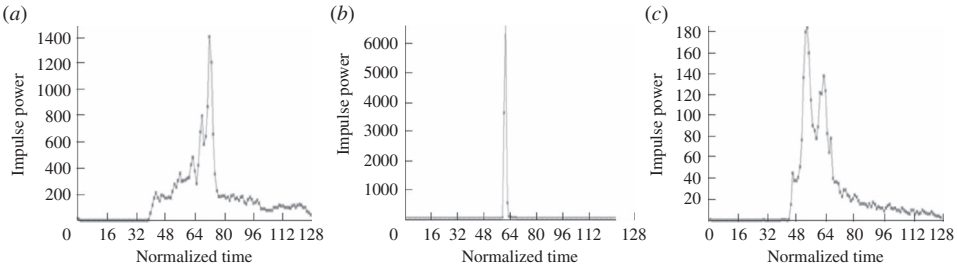

Figure 1. Waveforms in the coastal zone and inland waters: (*a*) combined reflection from land and water, (*b*) quasi-specular coherent reflection from a smooth water surface in estuaries and harbours, (*c*) in the presence of several highly reflecting objects.

developed for re-processing the altimetry data for the coastal zone (Anzenhofer *et al*. 1999, Deng and Featherstone 2006), large rivers (Koblinsky *et al*. 1993, Birkett 1998, Alsdorf *et al*. 2001, Benveniste and Berry 2004, Berry *et al*. 2005, Frappart *et al*. 2005, 2006) and lakes (Birkett 1995, Kostianoy *et al*. 2004, Cretaux *et al*. 2010). But there is still no standard technique which would allow use of a satellite database for the correct assessment of water level in a situation where the reflection from land strongly affects the received waveforms. There exist various retracking algorithms for determining the leading-edge arrival time of the reflected signal, for example threshold retracking and β-retracking (Martin *et al*. 1983, Davis 1997, Deng and Featherstone 2006, Lee 2008). In this article, we propose a method of regional adaptive retracking based on constructing a theoretical model describing the formation of telemetric waveforms by reflection from the piecewise constant model surface (figure 2) corresponding to the geography of the region. On this basis, we formulate the criteria for selecting the telemetric waveforms and justify the applicability of the threshold and the improved threshold retracking algorithm for determining the parameters of the underlying surface in inland water basins. Possible applications of these methods to the Gorky Reservoir on the Volga River are also considered.

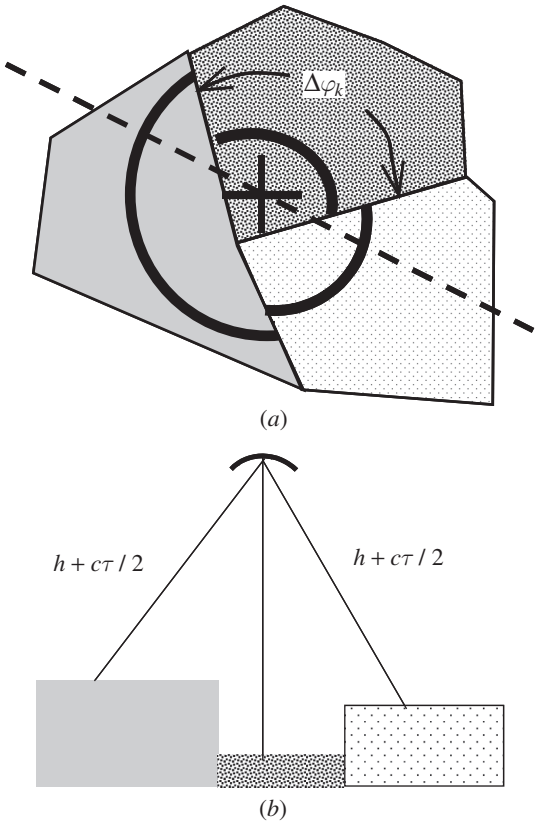

Figure 2. Piecewise constant model of underlying surface (+ denotes the position of nadir, the dotted line denotes the track of the satellite and the circle denotes the border of illuminated area at a given time). *a* is the top view and *b* is the side view.

For the open ocean conditions, the algorithm for determining the parameters of the underlying surface is based on the approximation of the altimeter waveform by the well-known Brown's formula (Brown 1977), derivation of which is based on the model of incoherent scattering of radio waves by a rough surface. Assuming that the radio waves coming from different parts of the surface are added incoherently, the power of the reflected signal is given by (Brown 1977, Barrick and Lipa 1985)

$$P(t) = P_0 \int\int_{\substack{\text{illuminated}\\ \text{area}}} \frac{G^2(\theta)\,\sigma(x,y,\theta)}{r^4} \mathrm{d}A \int_{-\infty}^{\infty} p\left(t_1 - \frac{2r}{c}\right) q\left(x, y, \frac{c}{2}(t - t_1)\right) \mathrm{d}t_1, \quad (1)$$

where G is the gain of the radar antenna; r is the distance from the radar to the elementary scattering area $\mathrm{d}A$ on the surface; x,y are Cartesian coordinates on the surface; θ is the angle, measured from antenna bore-sight axis to the area $\mathrm{d}A$ direction (see figure 1 in Brown (1977)); σ is the backscattering cross-section per unit scattering area; $p(t)$ is the radar system point-target response and $q(z)$ is the height probability density of specular points.

The transformations made in Brown (1977) for the case of small-angle approximation, small deviation of altimeter antenna axis from nadir ($\theta << 1$ and $\xi << 1$, see figure 1 in Brown (1977)) and model expressions for G, q, p and σ,

$$\begin{aligned} &\mathrm{G}(\theta) = \exp(-2\sin^2\theta/\gamma), \quad q(z) = \frac{1}{s\sqrt{2\pi}} \exp(-z^2/2s^2), \\ &p(t) = \frac{1}{\tau_i\sqrt{2\pi}} \exp(-t^2/2\tau_i^2), \quad \sigma = \sigma^{(0)} \mathrm{e}^{-\alpha\, tg^2\theta}, \end{aligned} \quad (2)$$

give the following expression for the waveform reflected from an infinite, statistically homogeneous underlying surface:

$$\begin{aligned} P\left(t - \frac{2h}{c}\right) = \frac{P_0\sigma^{(0)}}{2h^4} \left(1 + \mathrm{erf}\left(\frac{(ct - 2h)}{\sqrt{2}\sqrt{(2s)^2 + c^2\tau_i^2}}\right)\right) \\ \times \exp\left[-\frac{4}{\gamma}\sin^2\xi - \frac{c}{h}\left(t - \frac{2h}{c}\right)\left(\frac{4}{\gamma}\cos^2\xi + \alpha\right)\right] I_0\left(\frac{4}{\gamma}\sin^2\xi\sqrt{\frac{c}{h}\left(t - \frac{2h}{c}\right)}\right), \end{aligned} \quad (3)$$

where h is the mean distance from the satellite to the underlying surface. In the case of an inland waterbody, the altimeter footprint consists of several parts differing in heights and reflecting properties (e.g. water, swamp, dry land, etc.). They are schematically shown by different shades in figure 2. If we assume that the altimeter antenna axis is aimed strictly at nadir, then the contribution of each part to the reflection is described by the analogue of Brown's formula (see (3) for $\xi = 0$), which is multiplied by $\Delta\varphi_k/2\pi$ to take into account the contribution of the kth area:

$$P_k(\tau) = \frac{P_0\sigma_k^{(0)}}{4\pi h^4} e^{-\left(\frac{4}{\gamma} + \alpha_k\right)\frac{(c\tau - 2H_k)}{h}} \left(1 + \mathrm{erf}\left(\frac{(c\tau - 2H_k)}{\sqrt{2}\sqrt{(2s_k)^2 + c^2\tau_i^2}}\right)\right) \times \Delta\varphi_k. \quad (4)$$

Here the parameters with the index k: H_k, $\sigma_k^{(0)}$, α_k, s_k correspond to the level, scattering properties and roughness for a given (kth) part of the underlying surface (H_k is positive when the distance from the surface to the satellite is greater than the mean value and the surface level is lower than the mean value). In (4) we take into account the fact that at time $\tau = t - 2h/c$ the main contribution to the reflection from the kth illuminated area is given by an arc $\Delta\varphi_k$ (see figure 2) centred at the nadir point with coordinates x_N, y_N and determined by the condition of equality of the distance from the antenna to the kth piece of surface. The radius of the arc is equal to $\sqrt{h\,(c\tau - 2H_k)}$ and depends on the deviation of the surface level of this area from the average value. If the surfaces have different elevations, the beam will contact them at different angles; this is schematically illustrated by figure 2(*b*).

The total reflected power is the sum of the contributions from all the piecewise constant regions:

$$P(\tau) = \sum_{k=1}^{3} P_k(\tau). \tag{5}$$

Using (4) and (5) one can calculate the reflected waveforms and their changes when the satellite moves along the track.

3. An example of using the adaptive regional retracking method for determining the water level in the Gorky Reservoir

3.1 *Problems arising in determining the water level in the Gorky Reservoir using data from the Geophysical Data Record database of the Jason-1 satellite*

According to the NASA/CNES data (see figure 3), the water area of the Gorky Reservoir and that of the Volga River are each intersected by two ground tracks (pass 33 and pass 142) of altimetry satellites T/P and Jason-1,2 and several tracks of altimetry satellites European Remote Sensing (ERS) satellites (ERS-1 and ERS-2), Environmental Satellite (ENVISAT), Geodetic Satellite (GEOSAT) and GEOSAT Follow-On (GFO).

We used data for the 142nd pass of Jason-1 (before orbit manoeuvre), which intersects the Gorky Reservoir in its northern part (figure 1), with the track length within the reservoir being about 15 km. The altimetry data of this track were compared with the measurements from the ground station in Yurievets (a small town on the banks of the Gorky Reservoir). At the first stage, the Geophysical Data Records (GDRs) of the Jason-1 (J1) satellite were processed. All the 20 Hz Jason-1 altimetry data available along the pass 142 were used and all that are available in the original altimetric database corrections were calculated (AVISO 1996, Picot *et al*. 2008). The 'wet' and 'dry' troposphere corrections were calculated using meteorological data (atmospheric pressure and air humidity) obtained from the nearest weather station. The DORIS ionosphere correction was used for correcting the altimetry measurements of reservoir surface height. The sea state bias correction was determined on the basis of model calculations. Corrections for the state of the underlying surface, 'inverse barometer' and oceanic and pole tides that are used for determining the oceanic levels need not be taken into consideration for inland waters. A similar procedure was used earlier for determining the hydrological regime of large rivers in South America, Africa and

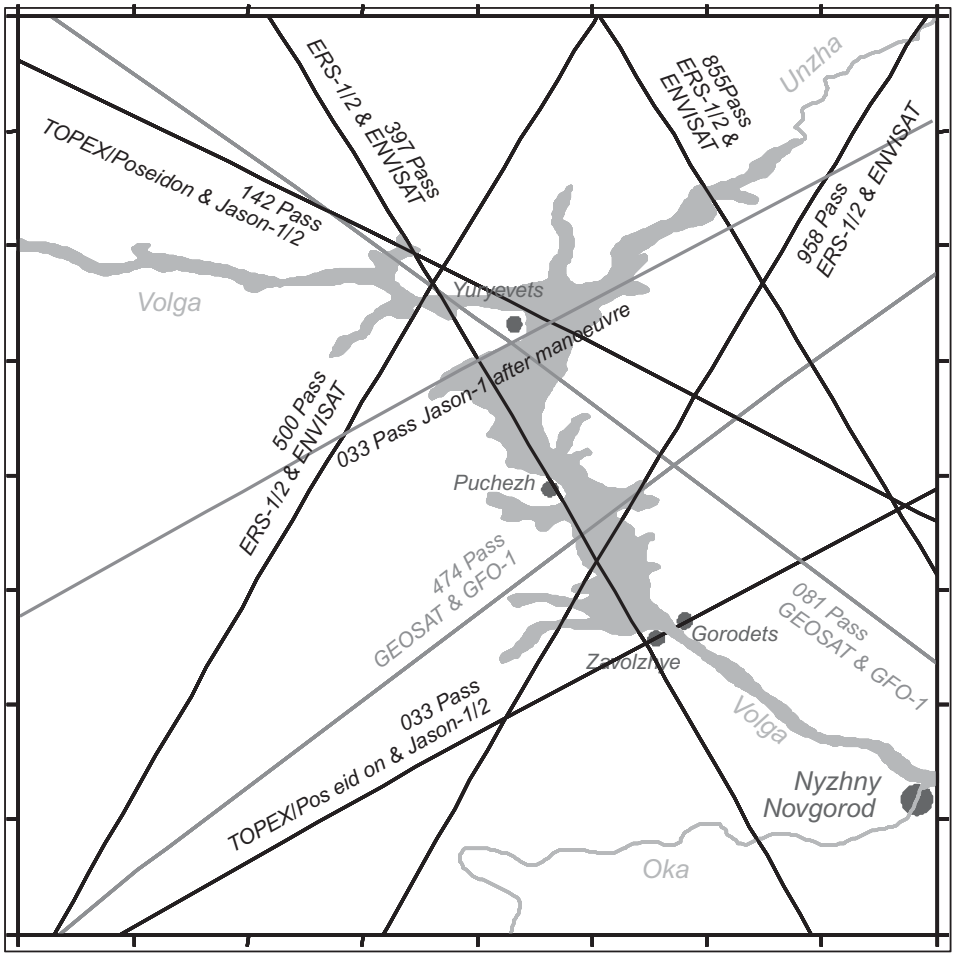

Figure 3. T/P, Jason-1, ERS-1/2, GEOSAT and GFO-1 tracks over the Gorky Reservoir water area.

Siberia (see, e.g. Campos *et al*. 2001, Birkett *et al*. 2002, Maheu *et al*. 2003, Kouraev *et al*. 2004), as well as for assessing the water level in the lower reaches of the Volga River (Lebedev and Kostianoy 2005). The efficiency of this procedure for large inland water areas was verified by comparing the results with the data of hydro-gauging stations.

Results of the data processing carried out following the described procedure were used to plot the water levels in the Gorky Reservoir with a resolution of 10 days in the period of 2002 to 2007 (grey squares in figure 4(*a*)). The results were compared with the measurement data obtained at the hydro-gauging stations of the State observation network (solid line in figure 4(*a*)). The correlation coefficient of altimetry data and *in situ* measurements is about 0.33 (figure 4(*b*)). The poor correlation between satellite and ground-based measurements is explained by significant loss of data and large errors caused by the shortcomings of a direct application of the altimetry algorithms

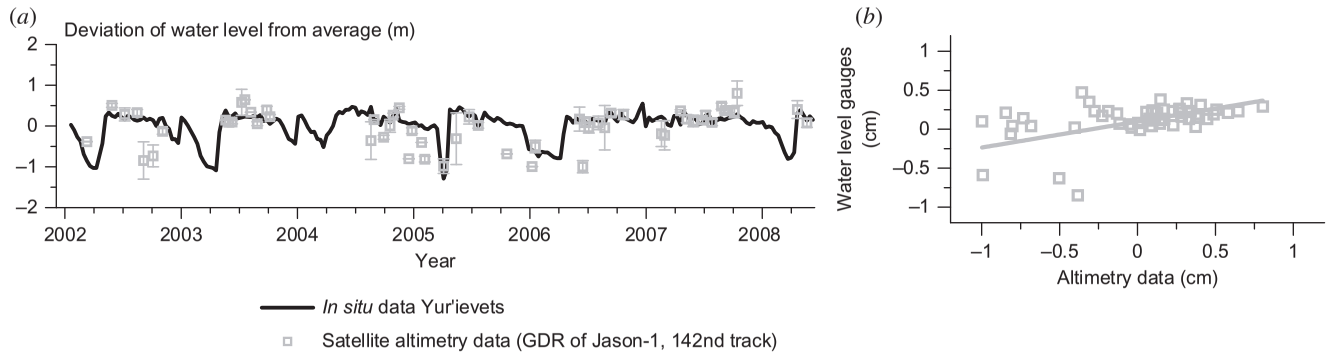

Figure 4. Water level dynamics in the Gorky Reservoir: (*a*) high-resolution altimetry data for the 142nd track of T/P and Jason-1 satellites (squares) and meteorological data from Yurievets station (solid line) and (*b*) normalized deviation from the mean water level (squares) and the best fit (straight line).

for water level retrieval designed for large water areas (oceans and seas) to middle-size water basins, in which the footprint of a radio-altimeter largely falls on the land.

To clarify the causes of significant errors, we analysed the waveforms of the reflected pulses received by the altimetry antenna. The necessary data were taken from the sensor geophysical data record (SGDR) database of the Jason-1 satellite. Special software was developed for the analysis of averaged reflected waveforms for high spatial resolution points with an averaging interval of 0.05 s. The software enables us to trace changes in the waveform as the nadir point is moving along the satellite track. Examples of varying waveforms for a point moving in the area marked by the white circle in the map are presented in figure 5.

The waveforms shown in the lower figure on the left represent the received reflected power as a function of time (the number of altimeter gates is laid off along the horizontal axis; one gate corresponds to the time interval $\mathrm{d}t_{\mathrm{g}} = 3.125$ ns; the power of the reflected signal is laid off along the vertical axis). An analysis of these waveforms suggests that the scatter in the water level data may be caused by drawbacks of the standard algorithm of computations in which the 32nd gate of the plots is regarded to be the arrival time of the reflected signal. However, one can see from the plot that the reflected signal may also arrive both before and after the mentioned gate, whereas the error of one gate leads to the error in the water level measurements of $\mathrm{d}t_{\mathrm{g}} \times c_{\mathrm{light}}/2 \approx 50$ cm.

Besides, the hydrometeorological regime of the Gorky Reservoir has a strong seasonal variability. In the winter, lasting from November to April, the entire water area is covered by ice and a snow layer, while the average date of freezing is November 22 (usually between November 7 and December 7) and the average date of clearing of the ice of the lake part of the reservoir is May 3 (usually between April 18 and May 18). The summer season, when the water area is free of ice, lasts from May to October. Examples of Jason-1 Ku-band waveforms for winter and summer seasons are given in figure 6.

In the winter (figure 6(*a*)), the waveforms are more or less regular and are fit for ice retracking. The summer waveforms (figure 6(*b*)) are complex, they can have quasi-specula or multiple quasi-specula components, etc. Brown's (1977) formula is not typically valid for approximation of such waveforms and an adaptive retracking algorithm is required.

3.2 *Piecewise constant model of telemetric pulse scattering for the Gorky Reservoir and its neighbourhood*

For the calculation of telemetric waveforms within the framework of equations (4) and (5), the underlying surface near the 142nd track of Jason-1 and T/P satellites (figure 7(*a*)) was approximated by the piecewise model depicted in figure 7(*b*), in which water and land have been shown by different shades. Note that our field studies revealed a specific feature of the Gorky Reservoir water area that could significantly influence the reflected waveforms. The 20–30 m wide smoothed regions (light-grey stripes in figure 7(*b*)) were regularly observed near the coastline, which were evidently caused by high concentrations of surface-active substances associated with economic activities. Such smoothed regions are known to give rise to peaks in telemetric pulses (Tournadre *et al*. 2006).

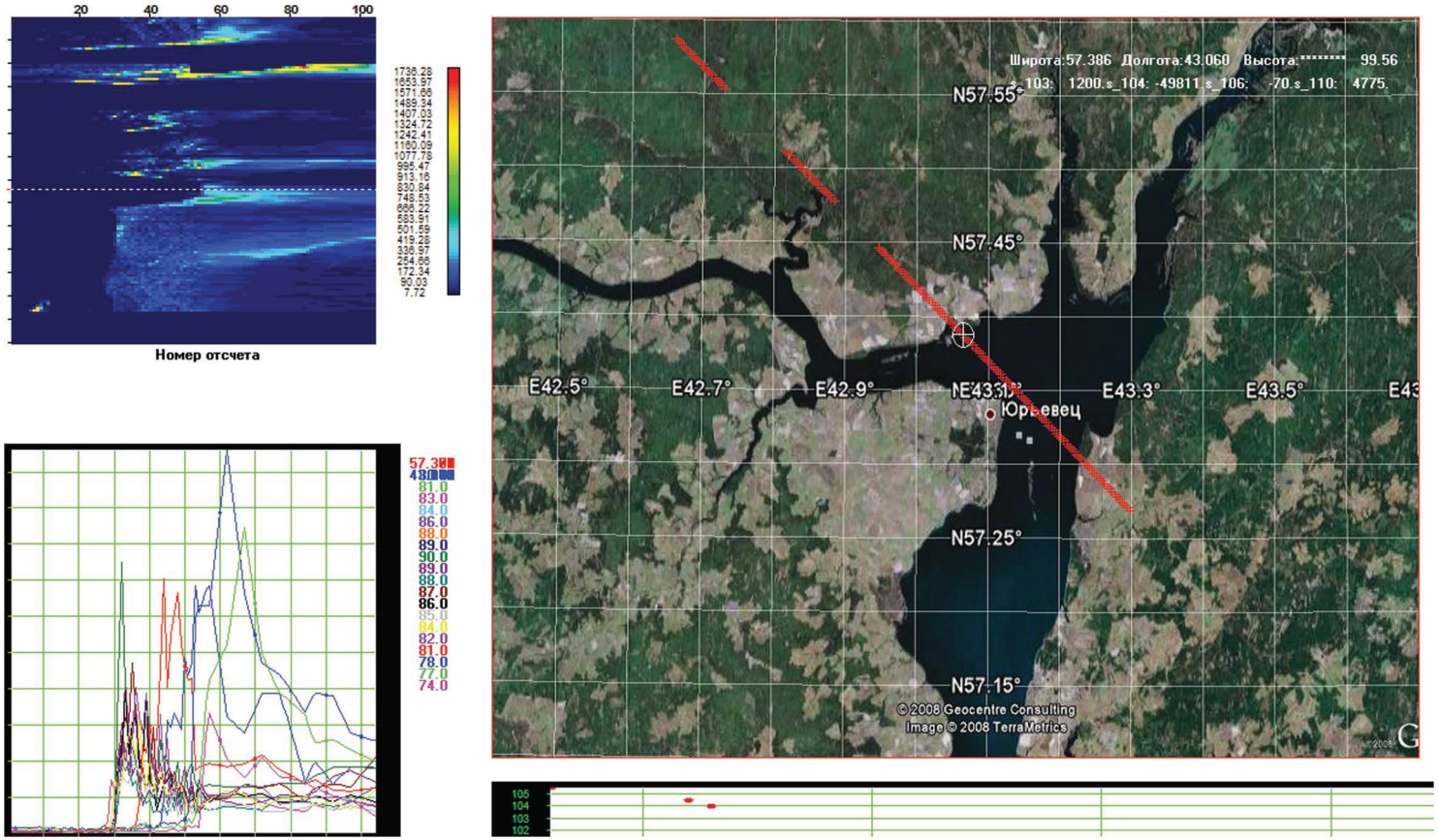

Figure 5. Copy of software monitor with examples of reflected waveforms from the SGDR base of Jason-1.

For an analysis of the contribution of slicks, let us transform the expression (1) with allowance for the simplifying assumptions adopted in Section 1. Then, (1) takes on the form of

$$P_i(\tau) = \frac{P_0}{\sqrt{2\pi}h^4} \iint \frac{\sigma^{(0)}}{\sqrt{(2s)^2 + c^2\tau_i^2}} \mathrm{e}^{-\left(\frac{4}{\gamma}+\alpha\right)\frac{\rho^2}{h^2}} \mathrm{e}^{-\frac{\left(c\tau - 2H - \rho^2/h\right)^2}{\left(8s^2 + 2c^2\tau_i^2\right)}} \mathrm{d}A. \tag{6}$$

In this expression, the parameters of the surface are functions of coordinates, $\rho^2 = (x - x_\mathrm{N})^2 + (y - y_\mathrm{N})^2$, x_N, y_N are the coordinates of a nadir point. Note that the slick

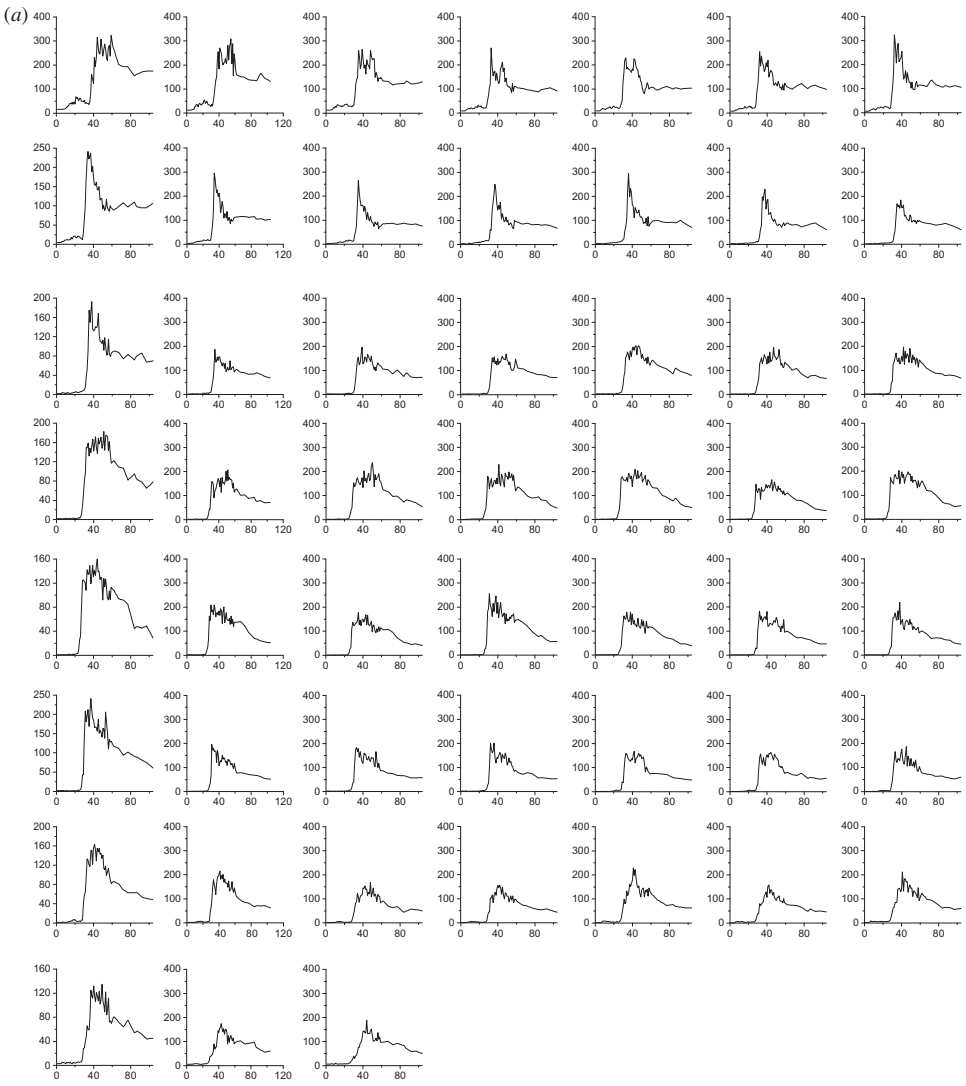

Figure 6. Waveforms of 20 Hz telemetric pulses for the 142nd track of Jason-1 satellite for the Gorky Reservoir: (*a*) 'winter' (25 March 2005) and (*b*) 'summer' (5 June 2006).

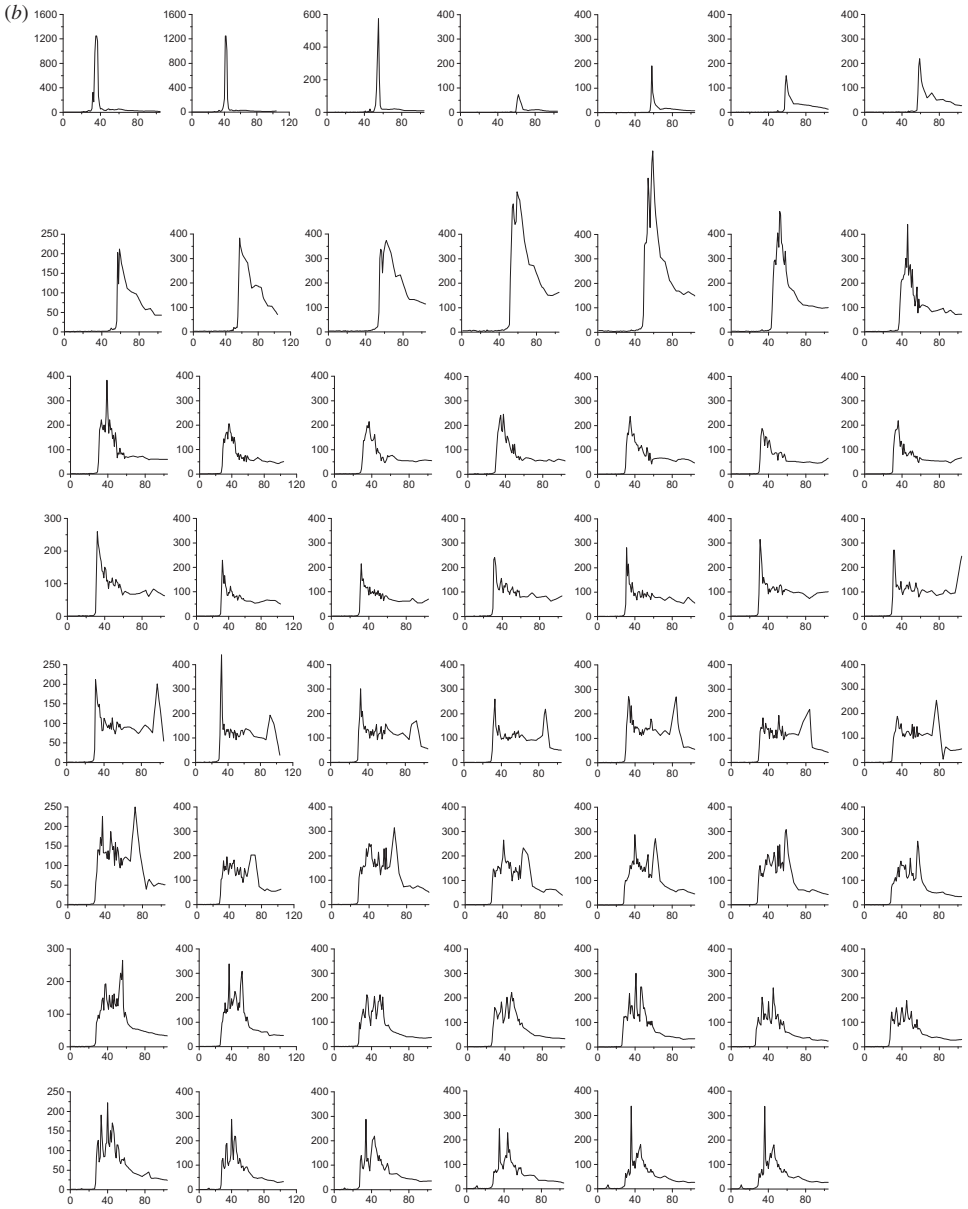

Figure 6. (*Continued*.)

water surface is almost smooth, so $\sqrt{8s^2 + 2c^2\tau_i^2} \approx \sqrt{2}\,c\tau_i$. For sufficiently short probe pulses, when the inequality $\left(\frac{4}{\gamma} + \alpha\right)\frac{\sqrt{2}c\tau_i}{h} << 1$ is valid, the second exponential in (6) represents a peak function with the maximum at $c\tau - 2H = \rho^2/h$, which enables one to take the other factors outside the integral by setting them as equal to the value

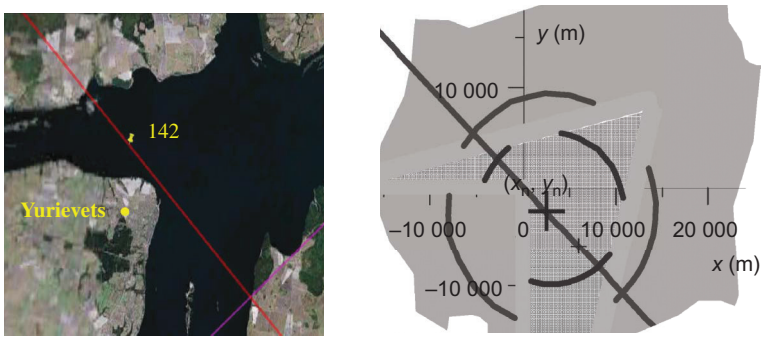

(*a*) (*b*)

Figure 7. (*a*) Map of the Gorky Reservoir near the town of Yurievets (the straight line denotes the 142nd track of Jason-1 satellite) and (*b*) piecewise constant model of the underlying surface: dotted shade denotes water, dark grey denotes land and light grey denotes coastal slicks).

at this point. Taking this into consideration, we can simplify this expression, then for narrow slicks extending along the coastline (coastal slicks), we obtain

$$P_{\mathrm{sl}}(\tau) = \frac{P_0 \sigma_{\mathrm{sl}}^{(0)} d_{\mathrm{sl}}}{\sqrt{2\pi} h^4 c\tau_i} \mathrm{e}^{-\left(\frac{4}{\gamma}+\alpha_{sl}\right)\frac{c\tau-2H_{\mathrm{water}}}{h}} \int_C \mathrm{e}^{\left\{-\left(c\tau-2H_{\mathrm{water}}-\frac{(x(l)-x_{\mathrm{N}})^2+(y(l)-y_{\mathrm{N}})^2}{h}\right)^2 \Big/ 2c^2\tau_i^2\right\}} \mathrm{d}l, \tag{7}$$

where $y = y(l)$, $x = x(l)$ is the equation of the coastal line C and d_{sl} is the width of the slick.

The reflected power received by the altimeter's antenna is the sum of the contributions from water and land described by (4) and the contribution of coastal slicks (7):

$$P(\tau) = P_{\mathrm{water}}(\tau) + P_{\mathrm{land}}(\tau) + P_{\mathrm{sl}}(\tau). \tag{8}$$

The parameters in formulas (4) and (7) are determined by the properties of the reflecting surface. For the water surface: elevation H is the water level, s is an SWH and σ is determined by the wind speed. For the land surface, H is determined by topography, s is surface roughness and σ is determined by the reflecting properties of the land. The model was constructed assuming that parameters of land are fixed, and the characteristics of surface water (water level, wave height and roughness) are variable and must be determined using the retracking algorithm.

For the case of underlying surface in the vicinity of the 142nd Jason-1 pass, we suggested a simplified piecewise constant geographical model of reflecting surface for Gorky Reservoir (compare figures 7(*a*) and (*b*)). The main simplification concerned the model of the land, which was supposed to have a constant height $H = 20$ m (an average height of the area according to Global Land One-km Base Elevation (GLOBE 1999) project; see figure 8). The shorelines were modelled by straight lines: $y = 0$ for $x < 0$, $x = 0$ for $y < 0$, $y = 0.25x + 5400$ for $-21\,600 < x < 14\,240$ and $y = 4x - 48\,000$ for $0 < x < 14\,240$.

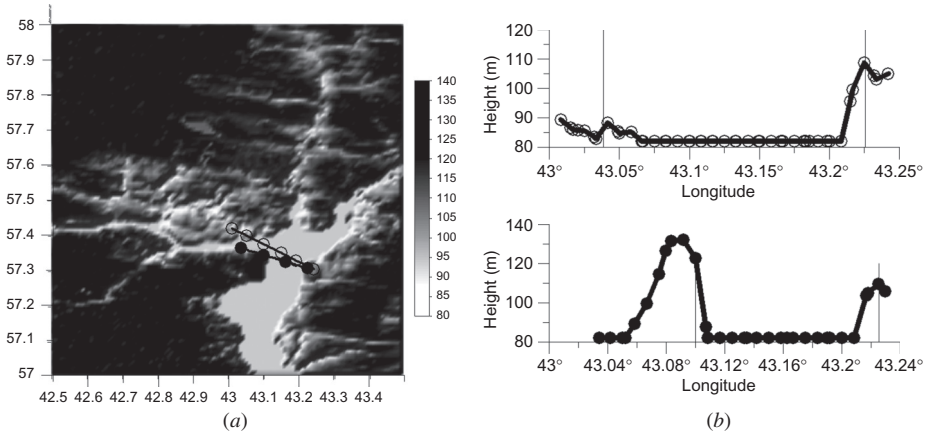

Figure 8. (*a*) Topology of the surface area near the Gorky Reservoir, taken from the database http://www.ngdc.noaa.gov/mgg/topo/globe.html. (*b*) The top and bottom figures on the right correspond to the lines with open and dark circles in (*a*), respectively.

Then, based on formulas (4), (7) and (8), the reflected waveforms for the 142nd Jason-1 track were calculated. The arcs $\Delta\varphi_k$ in (4) were calculated numerically for different times as the satellite moves along the track.

The contributions of water surface reflections to the telemetric waveforms were modelled assuming that the water level was spatially homogeneous over the reservoir. For determining parameter s, one needs to know the significant wind wave height found from data on the wind speed and direction measured at the Yurievets weather station (57° 20′ N 43° 07′ E); see figures 9(*a*) and (*b*). It is worth noting that the wind speed in the reservoir water area does not coincide with the wind speed measured at the coastal weather station in Yurievets. Special *in situ* measurements showed that wind speed in the water area is 1.5–2 times that on the coast.

The SWH was estimated from the empirical relation obtained by generalizing the measurements on Lake Ontario (Donelan *et al*. 1985):

$$\mathrm{SWH} = 0.2074\frac{U_{10}^2}{g}\Omega^{-1.55}, \tag{9}$$

where $\Omega = U_{10}/c_\mathrm{p}$ is the parameter characterizing wave height age, U_{10} is the wind speed at the height of 10 m and c_p is the phase velocity of wind-wave spectral peak. Donelan *et al*. (1985) showed that Ω is related to fetch x by the empirical formula

$$\Omega = 22\left(\frac{gx}{U_{10}^2}\right)^{-0.33}. \tag{10}$$

For an estimation of the statistics of surface waves, we calculated the angular distribution of fetches as a function of wind direction for the average point of the 142nd track of the altimetry satellites in the reservoir water area. The reservoir is anisotropic because of its elongated shape and the maximum fetch is attained with a south-southwest wind (figure 9(*c*)).

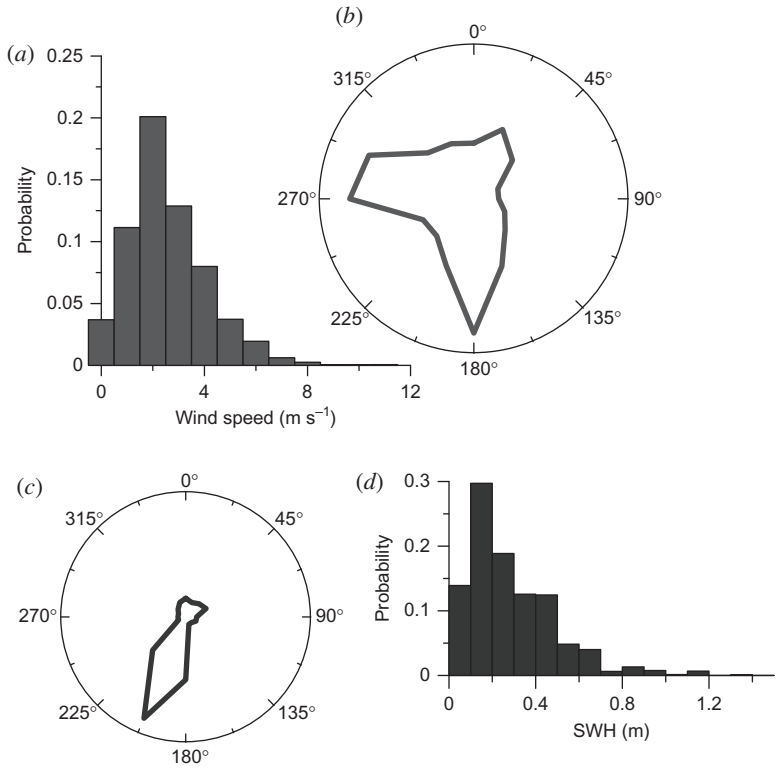

Figure 9. (*a*) Wind speed and direction in the summer of 2008–2009 (Yurievets weather station, 57° 20′ N, 43° 07′ E), (*b*) statistics of wind waves (according to field measurements on 29 July 2009), (*c*) angular distribution of the accelerations for the corresponding wind direction and (*d*) histogram of SWH (based on field measurements on 29 July 2009) for the mid-point of the track 142 of Jason-1.

Using histograms of wind speed distribution obtained at the Yurievets weather station taking into consideration the coefficient of the speed of wind from land to the reservoir water area, as well as histograms of the angular fetch distribution, we calculated the statistics of the SWHs in the Gorky Reservoir in the summer period using formulas (9) and (10). The histogram of wave height distribution is presented in figure 9(*d*). Calculation of the statistical expectation shows that the average wave height in the Gorky Reservoir in the summer period is very small, about 0.28 m.

Reflective properties of land, water and slicks are not exactly known for the region considered. However, taking into account the fact that the ratio of the reflection coefficients rather than their absolute values is important for the construction of waveforms, we choose the coefficients from physical considerations: for land $\sigma^{(0)} = 20,\ \alpha = 10$; for water $\sigma^{(0)} = 50,\ \alpha = 10$; for coast slicks $\sigma^{(0)} d_{\mathrm{sl}} = 0.5,\ \alpha = 1000$. The parameters specific to the radar altimeter were set equal to $\gamma = 0.0005, \tau_i = 0.425\,T$, where $T = 3.125 \times 10^{-9}$ s – the point target response 3 dB width.

Choosing parameters of equations (4), (7) and (8) in conformity with the above estimates, we calculated the waveforms of telemetric pulses. Our calculations correspond to the summer period. The winter case requires special consideration, since the conditions are quite different. In winter the water is covered with ice and snow, and the land

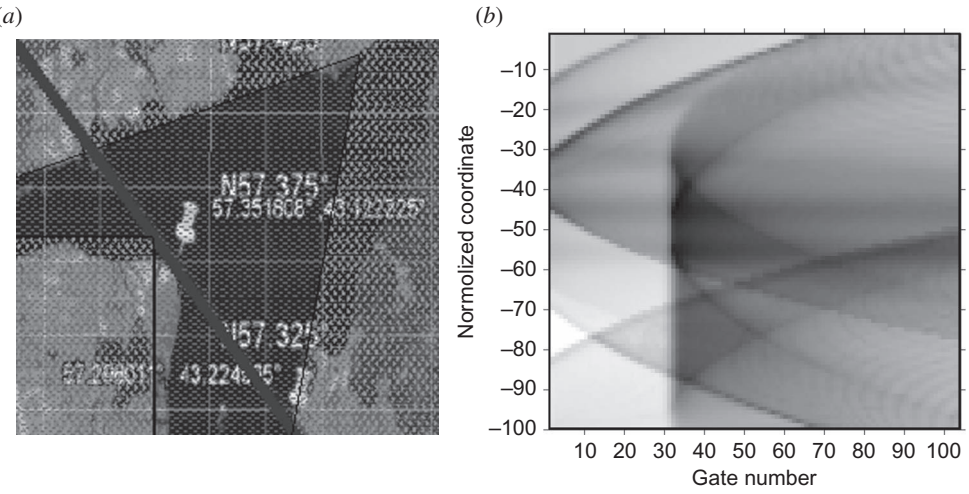

Figure 10. Model waveforms of reflected pulses for the Gorky Reservoir: (*a*) model map near the 142nd track of Jason-1 and (*b*) diagram of model waveforms (vertical denotes normalized coordinate along the 142nd track computed from the upper left corner of image (*a*)).

is also covered with snow, whose thickness can reach 1–2 m. As a result, the waveforms from the area considered are more similar to the ocean ones (see figure 6(*a*)).

The calculated summer model waveforms reflected from the surface close to the Gorky Reservoir are shown in figure 10. The results are presented in figure 10(*b*) as a histogram of telemetric waveforms (the coordinates are: time–distance along the track). Time is measured in units of telemetry gate (3.125 ns), and distance in terms of counts along the track (700 m). The complex form of the images reflects the complexity of the calculated model waveforms. Their characteristic features are parabolic singularities corresponding to the reflection from the coast and scattered on the slicks near the coast. By virtue of the small value of the average SWH (28 cm) the waveforms have an extremely narrow leading edge corresponding to less than 1 telemetry gate.

Based on these peculiarities of the calculated waveforms, we set the validity criteria for waveforms in the regional retracking algorithm as follows.

1. To determine the water level, one should take the waveforms from the 43.14–43.22 E section of the Gorky Reservoir (the lower half of the chart in figure 10(*b*) corresponding to the region between the marks in figure 10(*a*)), because only in this region can we reliably distinguish the signal reflected from water: the leading edge of this pulse falls on the 32nd remote gate, where it was placed purposefully in the calculations in accordance with signal processing on the satellite (the model reflected power arriving before the 32nd gate is connected with reflection from higher parts of the surface).
2. The deviation of the water level from an average value by more than 2 m should be considered erroneous.

For the valid waveforms, we propose the following regional retracking algorithms appropriate for the Gorky Reservoir for track 142, including two steps. At the first step, we estimate a tracking point determined by a definite threshold. The second

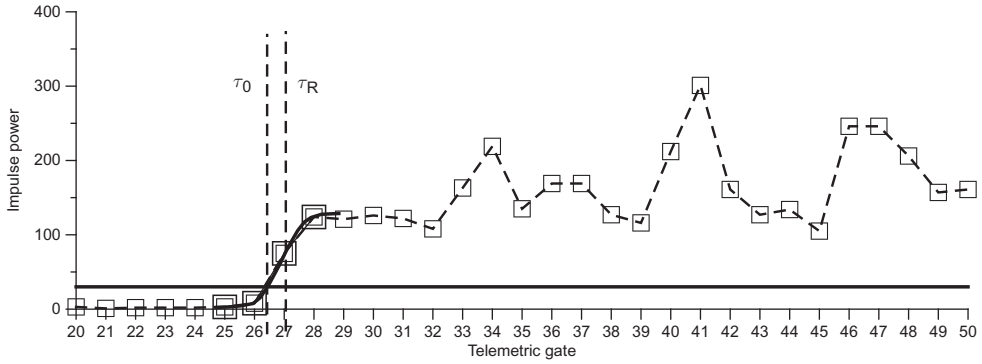

Figure 11. An example of a waveform from SGDR of Jason-1, cycle 162, track 142, Ku band (solid line denotes threshold power, τ_0 denotes the tracking point for threshold retracking and τ_R denotes improved threshold retracking).

step is refinement of the estimates: four points in the neighbourhood of the threshold (figure 11) are fitted by the error function (taking into account the analytical results):

$$A\left(1 + \mathrm{erf}\left(\frac{\tau - \tau_R}{S}\right)\right). \tag{11}$$

The parameters A, τ_R and S are retrieved from an optimization algorithm (by minimizing root mean square deviations). A possibility of approximating the leading edge of the part of the waveform reflected from the surface of the reservoir by the error function has been shown above, within the framework of the theoretical model. Indeed, the exponent on the right-hand side of equation (4) is a smooth function compared to the error function, hence the rise in pulse power near the leading edge may be considered to be specified by the error function. An improved retracking (see figure 11) gives a better value for the tracking point (the middle of the leading edge of the waveform reflected by water). Only the choice of an adequate optimization technique impedes application of the described method. Note that when the time of pulse arrival is found by a standard algorithm, the obtained tracking point is in the 32nd gate of the chart (figure 11), leading to errors in the arrival time of five gates and a 2.5 m error in determining the water level!

To conclude this section, we formulate the following basic principles of the proposed algorithm of regional adaptive retracking, which may be employed for inland as well as for coastal waters.

1. Constructing a regional model of reflecting surfaces (a piecewise constant one).
2. Solving a direct problem, modelling waveforms within the model.
3. Imposing restrictions and validity criteria for the algorithm on the basis of waveform modelling.
4. Solving the inverse problem in two steps: step one – retrieving a tracking point by the threshold algorithm; step two – refinement of the tracking point and (possibly) estimating SWH by solving the optimization problem.

Note that a similar procedure can be used for constructing regional adaptive retracking algorithms for retrieving water level from satellite altimetry for sufficiently

complex areas. The surface is divided into fractions with constant parameters (for example, a coastal zone can be represented as three strips: sea, land and intermediate area). The contribution of the surface is a sum of contributions from the fractions calculated by the analytical formula (4). Then, based on the modelled waveform image, the validity criteria are imposed and retracking is improved step-by-step.

4. Application of the algorithm of regional adaptive retracking for calculating water level in the Gorky Reservoir: a comparison of the results of calculation with data observed at weather stations

In this section, the method of adaptive regional retracking, whose theoretical principles were considered above, is employed to calculate the water level in the Gorky Reservoir. According to the results presented in Section 2 and the criteria of selecting altimetry waveforms, we took for retracking the waveforms from the section of the Gorky Reservoir corresponding to 43.14°–43.22° west longitude. Furthermore, the waveforms were subjected to a two-step processing. At the first step, the algorithm of threshold retracking was used, when the arrival time of the reflected waveform was determined by the power excess over the threshold. The level of the threshold was varied, with data concentration being the best at about 30–50 units of dimensionless power. At the second step (improved threshold), the position (the middle of the leading edge of the reflected waveform) of the tracking point was determined more accurately by approximating the leading edge (four points near the threshold found at the first step) by the error function (11) and minimization of RMS deviations.

The results of calculating changes in the water level in the Gorky Reservoir by two-step retracking (dark grey squares) and their comparison with the measurements at the Yurievets weather station (solid line) and GDR base (light grey squares) are presented in figure 12. The obtained results were used to calculate the correlation coefficient of altimetry data for the 142nd track of the Jason-1 satellite and data of ground measurements (angular coefficient of the straight lines in figure 13), and to determine errors in assessing water level and the amount of valid points in the summer and winter seasons for different retracking algorithms (table 1). The analysis revealed a significant increase in the number of valid measurement points, as well as a much better correlation between satellite and ground-based data. For example, the correlation

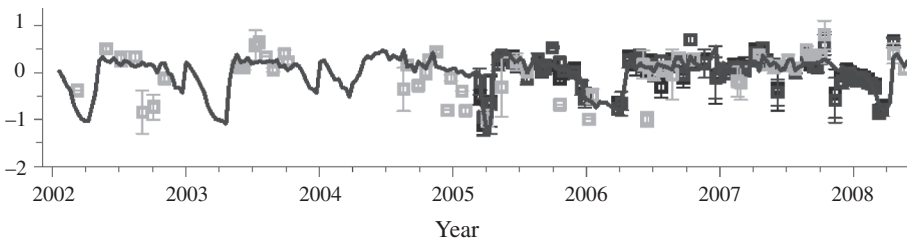

Figure 12. Water level variations in the Gorky Reservoir: GDR high-resolution data for track 142 of Jason-1 satellite (open squares), results of retracking SGDR base from Jason-1 satellite (filled squares) and meteorological data from Yurievets (solid line).

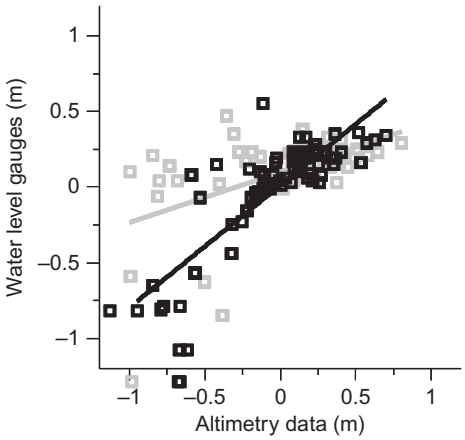

Figure 13. Normalized deviation from mean water level: GDR base is denoted by light grey squares and results of retracking SGDR base are denoted by dark grey squares. Best-fitting lines: light grey and dark grey, respectively.

Table 1. Standard deviation of the water level in the Gorky Reservoir and average number of valid points per month (for SGDR base regional retracking for 142nd track of Jason-1).

	Standard deviation of the water level (m)		Average number of valid points per month	
Method of retracking	Winter (November–April)	Summer (May–October)	Winter (November–April)	Summer (May–October)
GDR data	0.15	0.16	0.3	1.2
Retracking by the threshold method	0.15	0.13	1.5	2.0
Retracking by the improved threshold method	0.18	0.12	1.5	2.0

coefficient between altimetry data and measurements at the Yurievets weather station increased from 0.33 (with the standard algorithm of high spatial resolution) to 0.88 for the method of adaptive retracking.

5. Conclusion

An algorithm for assessing the water level in inland water basins and in the coastal zone of an ocean with an error of about 10–15 cm was constructed. The algorithm was tested at the Gorky Reservoir with complex topography, where the standard Ocean-1 algorithm is not applicable, resulting in significant data loss. A model of an average waveform reflected from a statistically inhomogeneous piecewise constant surface (topographic model) was constructed. The reflected power was calculated theoretically on the basis of the works of Brown (1977) and Barrick and Lipa (1985). The model was used to substantiate the criteria of data selection for the Gorky Reservoir. The water level was calculated by means of regional adaptive retracking of the SGDR

database for the Gorky Reservoir. It was shown that application of this algorithm greatly increases the number of included data and the accuracy of determining the water level.

The general principles of the proposed algorithm for a complicated area (coastal zone, inland waters and so on) are based on the calculations of the signal with allowance for inhomogeneity of a reflecting surface and may be used in different geographical regions.

Acknowledgements

The authors thank L. Filina and A. Panyutin for the hydrometeorological data provided. The work was done with financial support from the Russian Foundation for Basic Research (project No. 08-05-97016-r_povolzhye_a).

References

Alsdorf, D., Birkett, C., Dunne, T., Melack, J. and Hess, L., 2001, Water level changes in Large Amazon Lake measured with spaceborne radar interferometry and altimetry. *Geophysical Research Letters*, **28**, pp. 2671–2674.

Anzenhofer, M., Shum, C.K. and Rentsh, M., 1999, *Coastal Altimetry and Applications. Geodetic Science and Surveying*, Report No. 464 (Columbus: The Ohio State University), 40 pp.

AVISO/Altimetry, 1996, *User Handbook. Merged TOPEX/POSEIDON Products*, Report No. AVI–NT–02–101–CN. Edition 3.0 (Toulouse: AVISO), 201 p.

Barrick, D. and Lipa, B., 1985, Analysis and interpretation of altimeter sea echo. *Advances in Geophysics*, **27**, pp. 61–100.

Benveniste, J. and Berry, P., 2004, Monitoring river and lake levels from space. *ESA Bulletin*, **117**, pp. 36–42.

Berry, P.A.M., Garlick, J.D., Freeman, J.A. and Mathers, E.L., 2005, Global inland water monitoring from multi-mission altimetry. *Geophysical Research Letters*, **32**, L16401, doi:10.1029/2005GL022814.

Birkett, C., 1995, The global remote sensing of lakes, wetlands and rivers for hydrological and climate research. In *Proceedings of International Geoscience and Remote Sensing Symposium (IGARSS '95). Quantitative Remote Sensing for Science and Applications*, 10–14 July 1995, Firenze, Italy (IEEE), vol. 3, pp. 1979–1981. doi:10.1109/IGARSS.1995.524084.

Birkett, C.M., 1998, Contribution of the TOPEX NASA Radar Altimeter to the global monitoring of large rivers and wetlands. *Water Resources Research*, **34**, pp. 1223–1239.

Birkett, C.M., Mertes, L.A.K., Dunne, T., Costa, M.H. and Jasinski, M.J., 2002, Surface water dynamics in the Amazon Basin: application of satellite radar altimetry. *Journal of Geophysical Research*, **107**, 8059, doi: 10.1029/2001JD000609.

Brown, G., 1977, The average impulse response of a rough surface and its applications. *Antennas and Propagation, IEEE Transactions*, **25**, pp. 67–74.

Campos, I.O., Mercier, F., Maheu, C., Cochenneau, G., Kosuth, P., Blitzkow, D. and Cazenave, A., 2001, Temporal variations of river basin waters from Topex/Poseidon satellite altimetry. Application to the Amazon basin. *Earth and Planetary Sciences*, **333**, pp. 633–643.

Cretaux, J.-F., Calmant, S., Abarca Del Rio, R., Kouraev, A. and Bergé-Nguyen, M., 2010, LAKES studies from satellite altimetry. In *Coastal Altimetry*, S. Vignudelli, A. Kostianoy, P. Cipollini and J. Benveniste (Eds.) (Berlin: Springer-Verlag).

Davis, C.H., 1997, A robust threshold retracking algorithm for measuring ice sheet surface elevation change from satellite radar altimeters. *IEEE Transactions Geoscience and Remote Sensing*, **35**, pp. 974–979.

Deng, X. and Featherstone, W.E., 2006, A coastal retracking system for satellite radar altimeter waveforms: application to ERS-2 around Australia. *Journal of Geophysical Research*, **111**, pp. 1–16.

Donelan, M., Hamilton, J. and Hui, W.H., 1985, Directional spectra of wind generated waves. *Philosophical Transactions of the Royal Society London, Series A*, **315**, pp. 509–562.

Frappart, F., Do Minh, K., L'hermitte, J., Cazenave, A., Ramillien, G., Le Toan, T. and Mognard-Campbell, N., 2006, Water volume change in the lower Mekong from satellite altimetry and imagery data. *Geophysical Journal International*, **167**, pp. 570–584.

Frappart, F., Seyler, F., Martinez, J.M., Leon, J. and Cazenave, A., 2005, Floodplain water storage in the Negro River basin estimated from microwave remote sensing of inundation area and water levels. *Remote Sensing of Environment*, **99**, pp. 387–399.

GLOBE Task Team, Hastings, D.A., Dunbar, P.K., Elphingstone, G.M., Bootz, M., Murakami, H., Holland, P., Bryant, N.A., Logan, T.L., Muller, J.-P., Schreier, G. and MacDonald, J.S. (Eds.), 1999, *The Global Land One-kilometer Base Elevation (GLOBE) Digital Elevation Model, Version 1.0* (Boulder, CO: National Geophysical Data Center). Available online at: http://www.ngdc.noaa.gov/mgg/topo/globe.html

Koblinsky, C.J., Clarke, R.T., Brenner, A.C. and Frey, H., 1993, Measurement of river level variations with satellite altimetry. *Water Resources Research*, **29**, pp. 1839–1848.

Kostianoi, A.G., Zavialov, P.O. and Lebedev, S.A., 2004, What do we know about dead dying and endangered lakes and sea? In *Dying and Dead Seas. Climatic versus Anthropic Causes*, J.C.J. Nihoul, P.O. Zavialov and P.P. Micklin (Eds.), pp. 1–48 (Dordrecht: Kluwer Academic Publishers).

Kouraev, A.V., Zakharova, E.A., Samain, O., Mognard, N.M. and Cazenave, A., 2004, Ob' river discharge from TOPEX/Poseidon satellite altimetry (1992–2002). *Remote Sensing of Environment*, **93**, pp. 238–245.

Lebedev, S.A. and Kostianoi, A.G., 2005, *Satellite Altimetry of Caspian Sea* (Moscow: MORE Publ., Intern. Inst. of the Ocean) (in Russian), 366 p.

Lee, H.K., 2008, *Radar Altimetry Methods for Solid Earth Geodynamics Studies. Geodetic Science and Surveying*, Report No. 489 (Columbus, OH: The Ohio State University), 192 p.

Maheu, C., Cazenave, A. and Mechoso, C.R., 2003, Water level fluctuations in the Plata Basin (South America) from Topex/Poseidon Satellite Altimetry. *Geophysical Research Letters*, **30**, pp. 1143–1146.

Martin, T.V., Zwally, H.J., Brenner, A.C. and Bindschadler, R.A., 1983, Analysis and retracking of continental ice sheet radar altimeter waveforms. *Journal of Geophysical Research*, **88**, pp. 1608–1616.

Picot, N., Case, K., Desai, S. and Vincent, P., 2008, *AVISO and PODAAC User Handbook. IGDR and GDR Jason Products*. SMM–MU–M5–OP–13184–CN (AVISO). JPL D– 21352. Edition 4.1 (PODAAC), 130 p.

Tournadre, J., Chapron, B., Reul, N. and Vandemark, D.C., 2006, A satellite altimeter model for ocean slick detection. *Journal of Geophysical Research*, **111**, C04004, doi:10.1029/2005JC003109.